'Inverse Mapping' of Magnetospheric Optical Emission from Isolated Neutron Stars

P.O'Connor, A.Shearer, A.Golden

Computational Astrophysics Lab, N.U.I. Galway, Ireland

October 2002

Abstract

There are no fully self consistent theories of magnetospheric pulsar emission which can account for emission in the IR $\rightarrow$ UV energy range. The region within the magnetosphere where such emission arises is essentially unknown. This work is an attempt to place constraints on *possible* emission regions using a computationally intensive, 'inverse mapping' approach. If this approach is successful then the restriction of physical parameter space within the magnetosphere from which emission arises should make it viable to propose a more detailed physical model of emission. Initial results for the Crab pulsar (PSR 0531+21) are presented and compared with observational data.

1 Introduction

This work is primarily concerned with magnetospheric emission from IR $\rightarrow$ UV. Magnetosphereic pulsar emission theories and simulations have been worked on and developed by numerous individuals and groups over the last 30 years (e.g. [13], [1], [2], [12]). These theories divide according to emission location and the specific emission mechanism.

In approaching the problem of optical emission we assume there is a simple, global emission process occurring within the pulsar magnetosphere (modeled on synchrotron emission [16]). We simulate emission from a population of particles (number density given by the Goldreich-Julian density [8]) located at each point on a spherical grid decomposition of the magnetosphere. We determine the observed Stokes parameters (I, Q, U, V) as function of phase (ϕ) for all observer viewing angles (χ) and sample all possible values of dipole axis inclination (α) (see Figure 2).

Simulated light-curves are compared to observational data with those best matching the data selected. This process places a restriction on what inclination (α) and viewing angle (χ) combinations produce the emission we see while the origin of the phase resolved photons is used to give an inverse mapping into physical magnetosphere space. It is hoped that this technique may help to constrain an unknown - a hint at the spatial origin of where these emissions arise.

2 Basic Physical Model

Physically we are interested in modeling emission from an ensemble of synchrotron radiating particles with the underlying particle number density depending on location within the magnetosphere. The characteristics of synchrotron radiation from individual particles is well documented (e.g. [5], [4]) and exhibits in general elliptical polarisation which can be seen from the form of the amplitude $\mathbf{E_n}$ of the n^{th} harmonic of the electric vector [5]:

$$\mathbf{E_n} = \frac{\mu 2 e \omega_B}{\sqrt{3}\pi c r} exp(in\omega_B r/c) \frac{n}{sin^5\alpha}\left[(\xi^2+\psi^2)K_{2/3}(\eta)\mathbf{i_1} + i\psi\sqrt{(\xi^2+\psi^2)}K_{1/3}(\eta)\mathbf{i_2}\right] \tag{1}$$

where $\eta = n(\xi^2+\psi^2)^{3/2}/3sin^3\alpha$ with $\mathbf{i_1}$ and $\mathbf{i_2}$ being orthogonal vectors in a plane transverse to the observer direction. $\xi = \sqrt{1-\beta^2}$ with β being the particles velocity, ψ is the angle of closest approach of the particles trajectory to the observer line of sight and $K_{2/3}, K_{1/3}$ being Bessel functions of the second kind. In this situation linear polarisation occurs only when $\psi = 0$ - i.e. when the observers line of sight crosses the emission cone exactly (see figure 1).

In our case we have an optical power law spectral index which is obeyed for a relatively narrow band of frequencies [14]. Modeling of such an object necessitates the use of a *truncated power law* particle distribution. Emissivity parameters derived in [9] may be utilised in which:

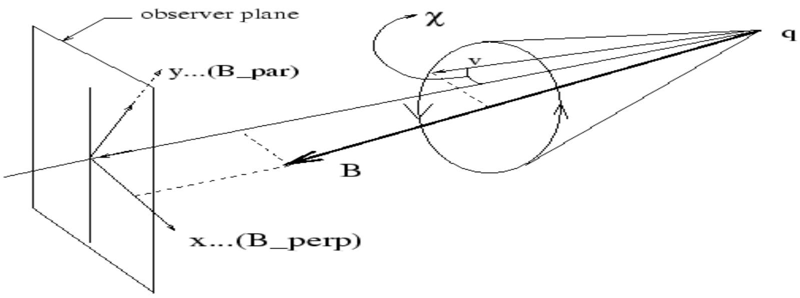

Figure 1: Polarisation projection for synchrotron radiation

$$\begin{aligned}
\eta_f &= \frac{A\mu e^2 c}{2\sqrt{2}}(\frac{3}{2})^{\gamma/2}\phi(\theta)(\nu_H sin\theta)^{(\gamma+1)/2}\nu^{-(\gamma-1)/2)}\mathcal{J}_{(\gamma+1)/2} \\
\eta_f^{(p)} cos2\lambda_f &= \frac{A\mu e^2 c}{2\sqrt{2}}(\frac{3}{2})^{\gamma/2}\phi(\theta)(\nu_H sin\theta)^{(\gamma+1)/2}\nu^{-(\gamma-1)/2)}\mathcal{L}_{(\gamma+1)/2} \\
\eta_f^{(p)} sin2\lambda_f &= \frac{A\mu e^2 c}{\sqrt{3}}(\frac{3}{2})^{\gamma/2}\phi(\theta)cot\theta(\nu_H sin\theta)^{\gamma/2+1}\nu^{-(\gamma/2)}\mathcal{L}_{(\gamma+1)/2} \\
&\times \left[\mathcal{R}_{(\gamma/2+1)} + [1+g(\theta)]\,(\mathcal{L}_{\gamma/2} - \frac{1}{2}\mathcal{J}_{\gamma/2})\right]
\end{aligned} \tag{2}$$

where $(\eta_f, \eta_f^{(p)} cos2\lambda_f, \eta_f^{(p)} sin2\lambda_f)$ can be related to stokes (I, Q, U, V) parameters and $\phi(\theta)$ is a representation of the pitch angle distribution function for the particle population. We extend these results to the case of a source rotating reference frame and derive the emission-polarisation tensor and finally the observed Stokes parameters for an observer at a viewing angle χ to the given pulsar.

3 'Inverse Mapping' Approach

The model used in this work can be divided into essentially two parts:

(a) the physical model of the emission process within the magnetosphere to create observer light-curves and polarisation data which has the following components:

- The magnetic field (**B**) is given by the Liénard-Wiechert potentials applied to a rotating dipole (the Deutsch field [3]):

$$\vec{B}(\vec{r}, t) = \frac{3\hat{r}(\vec{m}.\hat{r}) - \hat{m}}{r^3} + \frac{3\hat{r}(\dot{\vec{m}}.\hat{r}) - \dot{\vec{m}}}{r^2} + \frac{\hat{r}\times(\hat{r}\times\ddot{\vec{m}})}{r} \tag{3}$$

- This structure is sampled numerically by imposing a spherical grid throughout the magnetosphere (each grid point sampling an equal volume) and allowing each region to radiate independently.
- The local density of electrons/positrons is taken to be the Goldreich & Julian value: $N_{GJ} = \mathbf{\Omega}.\mathbf{B}/(2\pi ec)$.

- For the optical pulsars the total emission over the optical wavelength regions obeys a power law [7]. If the power for the overall spectral emission is η ($P(\omega) \propto \omega^{-\eta}$) then for a synchrotron source the source particle distribution is also a power law with:

$$N(\gamma)d\gamma = C\gamma^{-p}d\gamma, \quad \gamma_1 < \gamma < \gamma_2 \tag{4}$$

  where $\eta = (p-1)/2$. We model the local particle distribution as a **truncated power law** due to the narrow observed bounds of the spectral emission (see section 2).

- The local particle ensemble emits from each point on our grid. The radiation fields are calculated for such a population in co-rotation with the magnetosphere (relativistic aberration, beaming etc.) and the emission-polarisation tensor is used to determine the Stokes parameters which would be seen by a stationary celestial observer.

- The pitch angle distribution (PAD) of the emitting particles is critical in any consideration of synchrotron radiation (and is one of the great unknowns in this area). We have modeled various PAD's and present results for our 'best fitting' PAD.

(b) the 'inverse mapping' of this information:

- The simulated light-curves are compared to observational data via a χ^2 fit resulting initially in a restriction of (α, χ) space

- The phase resolved photon's originating locations are recorded and this is used to reconstruct the locations of emission within the magnetosphere for the best fit (α, χ) combinations.

- Presently the source regions are presented as a plot of the number of emitting points per radial bin as one moves through the magnetosphere to the light cylinder (see Figure 5).

In this way we can attempt to constrain (α, χ) parameter space and isolate regions within the magnetosphere likely to be the source of optical emission.

4 Geometry

To produce output to compare to observational data the simulations must be run over the parameter space associated with the geometry of neutron star emission. The neutron star spin ($\mathbf{\Omega}$) and magnetic (μ) axes can in theory be offset at any angle (denoted α) to each other i.e. α is such that $0 < \alpha < \pi$ (see Figure 2). The observer's geometry has a similar degeneracy as observer angle (χ) relative to the stars spin axis ($\mathbf{\Omega}$) can vary from $0 \rightarrow \pi$.

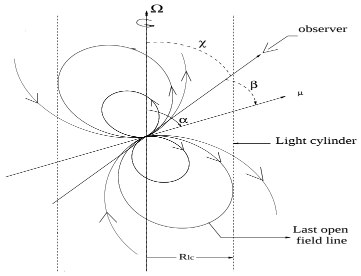

Figure 2: Generic picture of an inclined dipole

5 Results

Results may be grouped into a restriction of (α, χ) space (based on the comparison of our phase resolved values of (I, Q, U, V) to observations) and the subsequent localisation of emission regions within the magnetosphere for the resultant best fit (α, χ) combinations. This whole process is what we refer to as the 'inverse mapping' process. The Crab pulsar has by far the best data set available w.r.t. Stokes parameters [15] so the pulsar we model here is the Crab. We modeled emission in the optical in the U,B and V bands and show results here for the U band only which can be compared to Smith's [15] data.

5.1 Best fit to (α, χ)

There exists some restrictions on individual pulsar χ and α values from radio data and theory (e.g. [10], [11]) but these values do not in general agree with each other. In light of this no a priori assumptions are made as regards α or χ and simulations recorded the phase resolved Stokes parameters (I, Q, U, V) sampled for $1°$ increments in χ with $0° \leq \chi \leq 180°$ and for $10°$ increments in α for $0° \leq \alpha \leq 180°$.

We find that for the PAD envelope functions modeled (isotropic, circular and linear envelopes) the isotropic distribution fits the data best. We find that the different Stokes parameters result in different fits to (α, χ) space so what is required is a *global minimisation* of the best fit values for all (I, Q, U, V) taken together. A global minimisation for Stokes (I, Q, U, V) is shown in figure 3 giving the best-fit χ^2 values of our simulated lightcurves (U band) to the data. Lower values of χ^2 are best and the contour projection shows a distinct localisation of regions with best-fit χ^2 values ($\Rightarrow$ a restriction of (α, χ) parameter space).

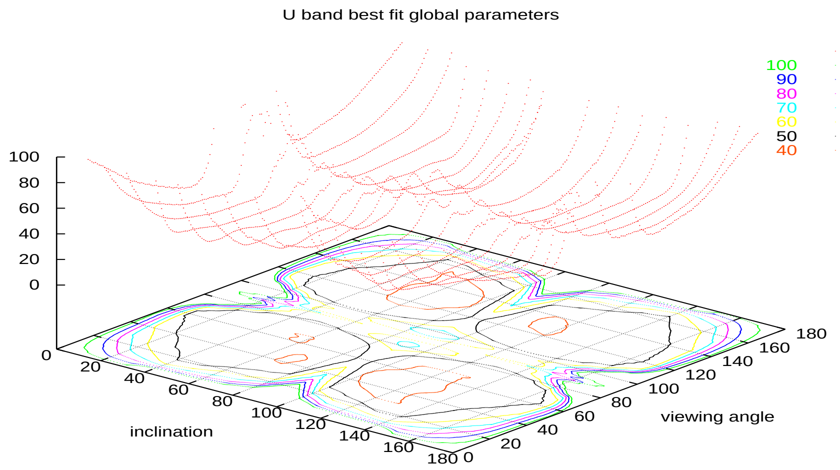

Figure 3: Global minimisation best fit χ^2 values to Stokes (I, Q, U, V) in U band for crab pulsar (lower values are best - see section 5.1)

5.2 Comparison with data

Smith [15] recorded Stokes (I, Q, U, V) for the Crab pulsar in 1988 and all results here use this data as a comparison data set. In the comparison with observations we use phase constraints for the Crab pulsar as in [6] and it is important to note that we have produced our simulation plots such that phase zero in our plots corresponds to the phase at the peak of the main peak shown in Smiths data therefore the

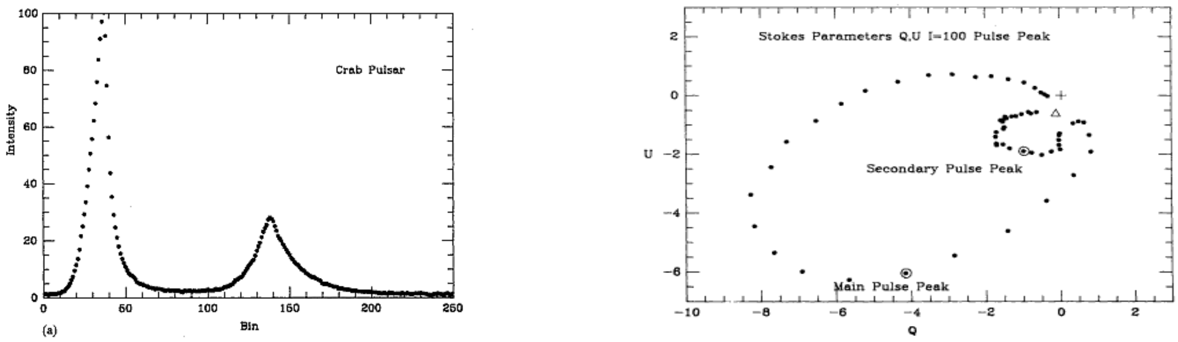

Figure 4: Observed light-curve and QU for the Crab [15]

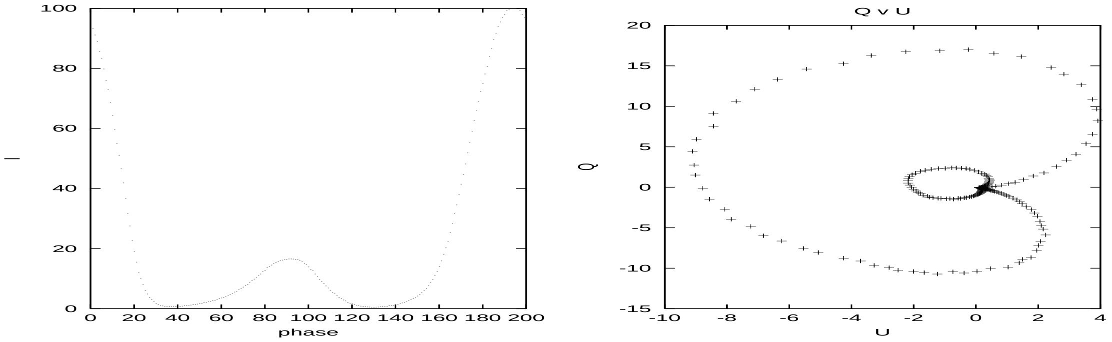

Figure 5: Simulation values of I and Q-U for the best fit $(\alpha, \chi) = (70°, 40°)$ (see section 5.2 for phase-alignments)

main peaks of the lightcurves in figures 4 and 5 are actually phase-aligned. From observations Stokes $V = 0$ at all phases and is reproduced as such in our simulations due to the symmetric nature of our pitch angle distributions; we are therefore left with Stokes (I, Q, U). Figure 4 shows observational data for the Crab and figure 5 shows results of our simulation for a selected (α, χ) combination of $(70°, 40°)$ *(which as can be seen from Figure 3 is in the globally minimised best fit region of* (α, χ) *parameter space)*. The results show that the morphology, phase offset and relative intensity of the double peaked lightcurve is reproduced although the simulation results have a much broader structure etc. The morphology of the roughly concentric U-Q plot is reproduced but with relative magnitudes and specific orientations of polarisation different from the data.Overall we take the morphological similarities of our Stokes (I, Q, U) as an indication of the promise of this 'inverse mapping' approach.

5.3 Inside the magnetosphere

For the selection of best fit $(\alpha, \chi) = (70°, 40°)$ we show a representation of the localisation of phase resolved emission regions within the magnetosphere. Figure 6 shows an inverse mapping of the originating locations of photons composing a 5% phase region around the main peak and a 5% phase region around the secondary peak respectively. The figures show in 2d the relative intensity contributions in spherical shells and cylindrical shells of 0.02 R_{lc} thickness and plotted in x-axis units where $R_{lc} = 1$. Currently our results indicate an emission location close to the neutron star - within $0.2R_{lc}$ of the surface.

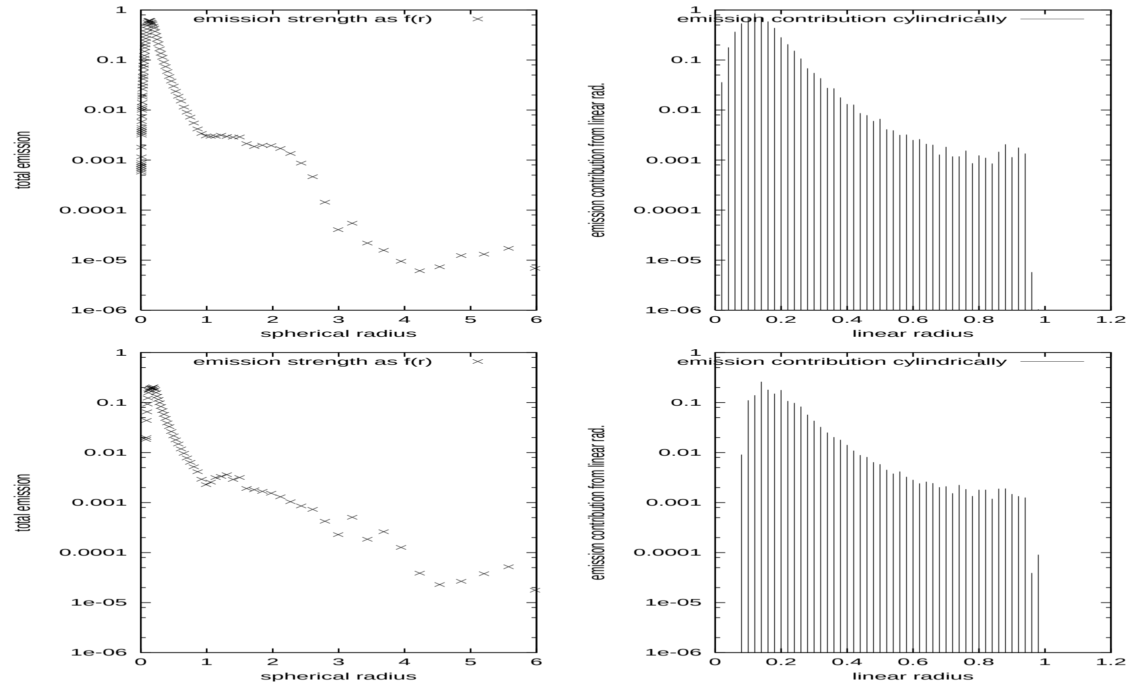

Figure 6: Inverse mapping of emission locations within magntosphere - top panel shows locations for main peak, lower panel for secondary peak (ordinate units are ratios of actual intensity to a fixed reference value)

6 Discussion / Conclusions

Although it reproduces only to first order the observational features mentioned above we interpret the morphological correlations of the simulations as indicative that this approach has potential. Even at this early stage we see that morphological similarities to the data result - via this inverse mapping approach - in vast restrictions on (α, χ) parameter space and also on physical location within the magnetosphere. Via a process of refining the physical model (section 2) the inverse mapping approach can be very useful.

Acknowledgments

P. O' Connor, A. Golden and A. Shearer are grateful for grants received from the National University of Ireland and also Enterprise Ireland.

References

[1] K. S. Cheng, C. Ho, and M. Ruderman. *ApJ*, 300:500–539, January 1986.

[2] J. K. Daugherty and A. K. Harding. *A&AS*, 120:C107–+, November 1996.

[3] A. J. Deutsch. *AnAp*, 18:1–+, January 1955.

[4] V. L. Ginzburg and S. I. Syrovatskii. *ARA&A*, 3:297–+, 1965.

[5] V. L. Ginzburg and S. I. Syrovatskii. *ARA&A*, 7:375–+, 1969.

[6] A. Golden. *Ph.D. Thesis*. NUIGalway, 1999.

[7] A. Golden, A. Shearer, and G. M. Beskin. *ApJ*, 535:373–378, May 2000.

[8] P. Goldreich and W. H. Julian. Pulsar Electrodynamics. *ApJ*, 157:869–+, August 1969.

[9] M. P. C. Legg and K. C. Westfold. *ApJ*, 154:499–+, November 1968.

[10] A. G. Lyne and R. N. Manchester. *MNRAS*, 234:477–508, October 1988.

[11] J. M. Rankin. *ApJ*, 352:247–257, March 1990.

[12] R. W. Romani. *ApJ*, 470:469–+, October 1996.

[13] M. A. Ruderman and P. G. Sutherland. *ApJ*, 196:51–72, February 1975.

[14] A. Shearer and A. Golden. *ApJ*, 547:967–972, February 2001.

[15] F. G. Smith, D. H. P. Jones, J. S. B. Dick, and C. D. Pike. The optical polarization of the Crab Pulsar. *MNRAS*, 233:305–319, July 1988.

[16] P. A. Sturrock. A Model of Pulsars. *ApJ*, 164:529–+, March 1971.